NeuroImage: Clinical 34 (2022) 103002

Contents lists available at ScienceDirect

NeuroImage: Clinical

journal homepage: www.elsevier.com/locate/ynicl

Diffusion tensor tractography of the fornix in cerebral amyloid angiopathy, mild cognitive impairment and Alzheimer's disease

Ibrahim Shaikh [a,b], Christian Beaulieu [b], Myrlene Gee [a], Cheryl R. McCreary [c,d,e,f], Andrew E. Beaudin [d,e], Diana Valdés-Cabrera [b], Eric E. Smith [c,f], Richard Camicioli [a,*]

[a] Department of Medicine, Division of Neurology and Neuroscience and Mental Health Institute (NMHI), University of Alberta, Edmonton, AB, Canada
[b] Department of Biomedical Engineering, University of Alberta, Edmonton, AB, Canada
[c] Department of Radiology, University of Calgary, Calgary, AB, Canada
[d] Hotchkiss Brain Institute, University of Calgary, Calgary, AB, Canada
[e] Department of Clinical Neurosciences, University of Calgary, Calgary, AB, Canada
[f] Seaman Family MR Research Centre, Foothills Medical Centre, Alberta Health Services, Calgary, AB, Canada

ARTICLE INFO

Keywords:
Cerebral amyloid angiopathy
Alzheimer's disease
Mild cognitive impairment
Diffusion tensor imaging
Fornix
Cognition

ABSTRACT

Purpose: Cerebral amyloid angiopathy (CAA) is a common neuropathological finding and clinical entity that occurs independently and with co-existent Alzheimer's disease (AD) and small vessel disease. We compared diffusion tensor imaging (DTI) metrics of the fornix, the primary efferent tract of the hippocampus between CAA, AD and Mild Cognitive Impairment (MCI) and healthy controls.

Methods: Sixty-eight healthy controls, 32 CAA, 21 AD, and 26 MCI patients were recruited at two centers. Diffusion tensor images were acquired at 3 T with high spatial resolution and fluid-attenuated inversion recovery (FLAIR) to suppress cerebrospinal fluid (CSF) and minimize partial volume effects on the fornix. The fornix was delineated with deterministic tractography to yield mean diffusivity (MD), axial diffusivity (AXD), radial diffusivity (RD), fractional anisotropy (FA) and tract volume. Volumetric measurements of the hippocampus, thalamus, and lateral ventricles were obtained using T1-weighted MRI.

Results: Diffusivity (MD, AXD, and RD) of the fornix was highest in AD followed by CAA compared to controls; the MCI group was not significantly different from controls. FA was similar between groups. Fornix tract volume was ~ 30% lower for all three patient groups compared to controls, but not significantly different between the patient groups. Thalamic and hippocampal volumes were preserved in CAA, but lower in AD and MCI compared to controls. Lateral ventricular volumes were increased in CAA, AD and MCI. Global cognition, memory, and executive function all correlated negatively with fornix diffusivity across the combined clinical group.

Conclusion: There were significant diffusion changes of the fornix in CAA, AD and MCI compared to controls, despite relatively intact thalamic and hippocampal volumes in CAA, suggesting the mechanisms for fornix diffusion abnormalities may differ in CAA compared to AD and MCI.

1. Introduction

Cerebral amyloid angiopathy (CAA) is defined pathologically by vascular deposition of β-amyloid peptides and clinically by its association with cortical cerebral macro-bleeds, microbleeds, and subarachnoid bleeds with associated superficial siderosis (Greenberg et al., 1995; Charidimou et al., 2017; Greenberg, 2018). Vascular changes (Peca et al., 2013) and cognitive impairment (Viswanathan et al., 2008) have also been reported in CAA. Alzheimer's disease (AD) is also defined by the deposition of amyloid, but in contrast to CAA, amyloid deposition is primarily in the cortical parenchyma. Microbleeds and white matter (WM) changes are also found in AD (Benedictus et al., 2013); however, CAA and AD are distinct disorders with different pathologies and clinical presentations.

Impairment in CAA mainly affects processing speed and executive function (Xiong et al., 2016; Case et al., 2016). In contrast, impairment in AD is defined by functionally significant cognitive decline, with early and prominent memory impairment (McKhann, 2011). Volumetric MRI studies in CAA and AD show both grey and white matter changes. Grey matter atrophy is prominent in AD (Knopman et al., 2016), most notably

* Corresponding author.
E-mail address: richard.camicioli@ualberta.ca (R. Camicioli).

https://doi.org/10.1016/j.nicl.2022.103002
Received 31 August 2021; Received in revised form 26 March 2022; Accepted 2 April 2022
Available online 4 April 2022

in the hippocampus. Atrophy in CAA shows global cortical thinning (Subotic et al. 2021) but less hippocampal volume loss than AD (Fotiadis et al., 2016). Hippocampal atrophy in CAA may differ depending on whether superficial siderosis is present (Kim et al., 2018). WM changes, including white matter hyperintensities (WMH) on T2-weighted fluid attenuated inversion recovery (FLAIR) images and atrophy, are noted in both CAA and AD; however, WM changes are greater in CAA compared to AD (Fotiadis et al., 2020).

Diffusion tensor imaging (DTI) tractography allows for a detailed characterization of WM tracts by isolating the tracts themselves and providing diffusion parameters reflective of tissue microstructure. Previous studies that examined WM changes in CAA using DTI found greater disruption of WM pathways were associated with processing speed (McCreary et al., 2020; Raposo et al., 2021). It has also been reported that posterior white matter connections, characterized by DTI, are impaired in CAA (Reijmer et al., 2016). A study that examined specifically defined tracts in CAA with autopsy correlations found diffusion changes in the anterior thalamic radiation and inferior longitudinal fasciculus that were associated with tissue rarefaction, myelin density, and white matter microinfarction (van Veluw, et al., 2019).

The fornix is a key hippocampal efferent tract that is affected in age-related cognitive decline (Fletcher et al., 2013), mild cognitive impairment (MCI) and AD (Tang et al., 2017) as well as in disorders with white matter involvement, such as multiple sclerosis (Valdés Cabrera et al., 2020). As such, the fornix is a potential neuro-modulatory therapeutic target in diseases and disorders such as AD (Senova et al., 2020). Given the importance of the fornix as a major connecting tract from the hippocampus, and its susceptibility to degeneration in AD and MCI, this study aimed to reliably characterize diffusion from this one structure, and compare changes in the fornix in CAA to disorders where degeneration of the fornix is better established. To our knowledge, there are no previous diffusion tensor tractography studies of CAA focussing on the fornix. Due to its small, curvilinear structure and proximity to adjacent cerebrospinal fluid (CSF), the fornix is difficult to measure in typically low-resolution DTI ($\sim$2x2x2 = 8 mm^3 isotropic voxels). The presence of atrophy associated with neurodegeneration makes this measurement even more challenging; however, a reliable tractography approach with high spatial resolution and CSF-suppression to minimize artifacts (Concha et al., 2005a,b) can better identify and measure diffusion parameters of the fornix.

Our primary objective was to use CSF suppressed diffusion imaging to examine the fornix in non-demented patients with probable CAA, patients with MCI and AD, and healthy controls. The correlation between fornix diffusion measures and hippocampus, thalamus, lateral ventricles, and WMH volumes were examined. We also explored the relationship between fornix diffusion measures and cognitive function. We hypothesized that the fornix would show diffusion changes in CAA, AD, and MCI relative to healthy controls, and that these changes would be associated with brain atrophy and cognitive impairment.

2. Methods

2.1. Participants

Participants were recruited as part of the Functional Assessment of Vascular Reactivity (FAVR)-II study across two sites in Alberta, Canada – Calgary and Edmonton. Probable CAA participants (N = 32), diagnosed by modified Boston criteria (Linn et al., 2010), were recruited from stroke prevention and cognitive and memory clinics coordinated through the Foothills Medical Centre in Calgary and the University of Alberta Hospital in Edmonton. Eligibility was based on presentation of a CAA-related syndrome and diagnosis according to the modified Boston criteria (Charidimou et al., 2017). Exclusion criteria for CAA included symptomatic intracerebral hemorrhage (ICH) in the previous 90 days, dementia, or living in long-term care.

Participants with AD (N = 21) and MCI (N = 26) were recruited from cognitive and memory clinics as well as community advertisement. Diagnosis of AD and MCI were made using the same criteria as previously described for a similar cohort (McCreary et al., 2020). Briefly, community-dwelling AD participants with mild dementia were diagnosed based on the National Institute on Aging-Alzheimer's Association criteria for clinically probable AD (McKhann et al., 2011). Participants with MCI were diagnosed according to National Institute on Aging criteria (Albert et al., 2011).

Healthy controls (N = 47) were recruited through spouses of patients seen at stroke and cognitive disorder clinics or from the local community through advertisements. All participants enrolled in the FAVR-II study did not have other neurological and psychiatric disorders, nor contraindications for MRI at 3.0 T. Additional self-reported controls (N = 21) were recruited as part of a normative aging study at the University of Alberta using the same imaging protocol. Informed consent was obtained from all participants in accordance with the University of Calgary and the University of Alberta research ethics boards and all research protocols were conducted according to the World Medical Association Declaration of Helsinki.

2.2. Cognitive Assessment

For participants enrolled in the FAVR study, standardized neuropsychological assessments were performed by qualified personnel. Assessments included the digit symbol substitution from the Weschler Adult Intelligence Scale (WAIS-III), Trail Making test parts A and B, Delis-Kaplan Executive Function System (D-KEFS) verbal fluency test, Rey Auditory Verbal Learning Test (RAVLT), Brief Visuospatial Memory Test – Revised (BVMT-R), and Montreal Cognitive Assessment (MoCA). Similar to a previous study (Subotic et al., 2021), neuropsychological raw test scores were converted to z-scores using published normative data with correction for age and education, then combined into domains of memory (average z-scores of delayed recall on the RAVLT and BVMT-R), executive function (average z-scores of D-KEFS letter fluency and Trail Making part B), and processing speed (average z-scores of Trail Making part A and WAIS-III digit substitution).

2.3. MR image acquisition

All participants were imaged using 3.0 T MRI scanners. Participants recruited in Calgary were scanned using a GE Discovery MR750 with a 32-channel head coil. Participants recruited in Edmonton were scanned on a Siemens MAGNETOM Prisma with a 64-channel head-neck coil. In order to minimize the deleterious effect of fast diffusing, isotropic CSF on tractography of the fornix (which is bathed in CSF), fluid-attenuated inversion recovery DTI (i.e. FLAIR-DTI) was used to null CSF signal in acquisition. It uses an inversion recovery pulse followed by an appropriate delay based on the T1 of CSF prior to the spin-echo diffusion sequence (Kwong et al., 1991), and has been shown to improve tractography of the human fornix (Concha et al., 2005a). The inversion recovery and delay time makes the TR and total acquisition time longer relative to regular DTI, but it can be limited by reducing the number of slices to cover only the fornix rather than whole brain.

2.3.1. Calgary

Fluid attenuated inversion recovery-DTI (FLAIR-DTI) images with a single shot, spin-echo echo planar imaging (EPI) sequence were acquired with 36 contiguous slices, 2.0 mm slice thickness (no gap) for a total coverage of 72 mm, 230 mm in-plane field of view (FOV); 128 × 128 acquisition matrix, acquired voxel size of 1.8 mm × 1.8 mm × 2 mm = 6.48 mm^3 which was reconstructed with interpolation resulting in 0.9 mm × 0.9 mm × 2.0 mm voxels, TR = 10000 ms, TE = 61.7 ms, TI = 2200 ms (to null CSF), 20 directions with b = 1000 s/mm^2, 5 b0 volumes (b = 0 s/mm^2) and SENSE with an acceleration factor of 2 for a scan time of 4:20 min. The imaging volume was oriented along the bicommissural line (AC-PC), and covered from the top of the corpus callosum to the

bottom of the temporal lobes to ensure full coverage of the fornix. Whole brain sagittal T1-weighted images were acquired using 3D-inversion prepared fast spoiled gradient echo (IR-FSPGR) with 256 slices, 1.0 mm slice thickness, 256 mm FOV, 256 × 256 acquisition matrix, voxel size of 1.0 mm × 1.0 mm × 1.0 mm = 1.0 mm^3, flip angle of 11°, TR = 7.5 ms, TE = 3.1 ms, TI = 400 ms, and SENSE with an acceleration factor of 1.5 for a scan time of 6:12 min. To assess WM disease, 2D FLAIR images were acquired with a 240 mm FOV, 3.0 mm slice thickness, 256 × 256 acquisition matrix, voxel size = 0.9 mm × 0.9 mm × 3.0 mm = 2.43 mm^3, TE = 140 ms, TR = 9000 ms. TI = 2250 ms, and flip angle = 125° for a scan time of 4:49 min.

2.3.2. Edmonton

Fluid attenuated inversion recovery-DTI images with single shot spin-echo EPI were acquired with 35 slices, 2.0 mm slice thickness (no gap) with a coverage of 70 mm, 240 mm FOV, 188 × 188 acquisition matrix, voxel size of 1.2 mm × 1.2 mm × 2.0 mm = 2.88 mm^3 zero-filled interpolated on scanner to 0.6 mm × 0.6 mm × 2.0 mm = 0.72 mm^3, TR = 9000 ms, TE = 70 ms, TI = 2300 ms (to null CSF), 20 directions with b = 1000 s/mm^2, 5 b0 volumes (b = 0 s/mm^2), GRAPPA acceleration factor of 2, and phase partial Fourier image reconstruction using 75% k-space coverage for a scan time of 4:11 min. The imaging volume included the top of the corpus callosum to the base of the temporal lobes, oriented along the bicommissural line (AC-PC) to allow full coverage of the fornix. Whole brain sagittal T1-weighted images were acquired using 3D-magnetization prepared rapid gradient echo (MPRAGE) with 208 slices, 0.85 mm slice thickness, coverage of 188 mm, 250 mm FOV, image matrix 288 × 288, voxel size of 0.85 mm × 0.85 mm × 0.85 mm = 0.61 mm^3 with no subsequent interpolation, TR = 1800 ms, TE = 2.37 ms, TI = 900 ms, flip angle 8°, and GRAPPA acceleration factor of 3 for a scan time of 3:39 min. For evaluation of WM disease, 2D FLAIR images were also acquired with 240 mm FOV, 3.0 mm slice thickness, 256 × 256 acquisition matrix, voxel size = 0.9 mm × 0.9 mm × 3.0 mm = 2.43 mm^3, TE = 120 ms, TR = 9000 ms, TI = 2500 ms, a flip angle of 165°, and a GRAPPA acceleration factor of 2 for a scan time of 2:44 min.

2.4. Volumetric analysis

Automated segmentation and volumetrics of subcortical brain regions, including hippocampus and thalamus, and ventricles was performed using the "recon-all" pipeline in FreeSurfer (v6.0) (Fischl, 2012) using T1-weighted images (Duchesne et al., 2019; Potvin et al., 2019; Smithet al., 2021). Intracranial volume (ICV) was also estimated (Fischl, 2012) by FreeSurfer. Left and right volumes were summed and reported as a percentage of the ICV (summed volume/ICV × 100%). FreeSurfer segmentation and parcellations were visually inspected for quality control. Four participants in the CAA group with ICH failed the quality control of the FreeSurfer output in that the surfaces generated for the hemisphere with the ICH were not reasonable. A visual review of the hippocampi on T1 images by an expert radiologist was performed to assess for symmetry between left and right subcortical structures. No notable asymmetry was found in these cases. To maximize the number of CAA participants in this study, the contralateral volume was doubled to estimate subcortical structure volume for these participants.

WMH volume for each participant was determined on FLAIR images by one of three trained readers using a semi-automated seed-based 3D region growing algorithm (Cerebra-Lesion-Extractor v1.1.2, Calgary Image Processing and Analysis Centre, University of Calgary, Alberta, Canada). To normalize for different head sizes, individual WMH volumes were also corrected to ICV followed by a log transformation to achieve a normal distribution.

2.5. Neuroimaging Assessment for CAA

Key neuroimaging markers of CAA including cerebral microbleeds (CMB), ICH, cortical superficial siderosis (cSS) with further classification to focal cSS (restricted to ≤ 3 sulci) or disseminated cSS (≥4 sulci), and WMH were defined according to the Standards for Reporting Vascular Changes on Neuroimaging (STRIVE) (Wardlaw et al., 2013) and evaluated for presence, number, and location by a qualified reader (a radiologist with greater than ten years of experience) on T1-weighted and FLAIR images.

2.6. DTI processing and tractography

All FLAIR-DTI images were examined for excessive subject motion and other artifacts. Diffusion tensor images were processed with ExploreDTI (v4.8.6) (Leemans et al., 2009) and included corrections for Gibbs ringing, subject motion, and eddy current distortions alongside tensor fitting using Robust Estimation of Tensors by Outlier Rejection. Deterministic tractography was also carried out in ExploreDTI, with a seed point resolution and step size matching the voxel size for each site and the following stopping criteria: a FA threshold of 0.15, a turning angle of 35°, and a minimum fiber length of 10 mm. All participants, regardless of group, were processed with the same protocol. Tractography was performed by the first author (IS), who was blinded to group classification until the fornix tracking was completed. Two types of regions of interests (ROIs) were utilized: 'AND' ROIs which include the fibers passing through them and 'NOT' ROIs which exclude the fibers passing through them. The ROIs were placed similar to previously published protocols for limbic system tracts (Concha et al., 2005a,b): 'AND' ROIs in the fornix body (coronal, roughly midway between crus and anterior commissure) to assure that fibers are passing between ventricles; and 'NOT' ROIs, as needed, to remove spurious anterior commissure and other callosal or thalamic fibers.

Stopping criteria and ROI placement were selected to yield reliable and consistent tracts over the entire cohort, prioritizing higher number of fornix fibers, zero to low number of spurious fibers, and low incidence of fiber disconnections. Spurious streamlines were removed based on a priori knowledge of the fornix location, and final tracts were reviewed by an experienced clinical neurologist (RC). To reduce multiple comparisons, both left and right fornix were kept together to yield tract volume, mean diffusivity (MD), axial diffusivity (AXD), radial diffusivity (RD), and fractional anisotropy (FA). Excellent intra-rater reliability (ICC ≥ 0.8) was found for the diffusion measures using a set of 16 images with a 2-week interval between ratings. Inter-rater reliability, assessed on the same set of images by two other raters (MG and DVC), was also excellent (ICC ≥ 0.8).

2.7. Statistical analysis

Statistical analyses were conducted using IBM SPSS Statistics for Windows (v26.0). Group demographics and MRI measurements, including volumes and WMH, were compared using one-way analysis of variance (ANOVA) for continuous variables and Chi-squared test for categorical variables. Fornix diffusion measures and volumes were compared using one-way analysis of covariance (ANCOVA), co-varying for age, and sex. A factor for site was also included in the model as the different acquisition parameters for DTI at each site necessitated a means to account for expected differences in diffusion measures. To identify group differences post-hoc, the Sidak correction for multiple comparisons was used. Relationships between diffusion measures and cognitive scores for the clinical groups were assessed using partial Pearson correlation, controlled for age, sex, site, and years of education. Similarly, relationships between diffusion measures and volumes for the clinical groups were assessed using partial Pearson correlation, controlled for age, sex, and site. Multiple comparisons correction for volumetric and diffusion measures as well as correlations was performed using the Benjamini-Hochberg False Discovery Rate (FDR) method with an FDR $p < 0.05$ resulting in an adjusted p-value threshold of ≤ 0.028.

3. Results

3.1. Participant characteristics

One hundred and forty-eight participants were recruited in this study. One CAA participant originally included had poor quality of diffusion data and was excluded from the study. Group characteristics, including cognitive scores, and MRI findings are presented in Table 1. Participants with CAA were older than the control ($p = 0.001$) and AD ($p = 0.03$) groups, but of a similar age to the participants with MCI ($p = 0.6$). Hypertension and microbleeds were more frequent in CAA participants compared to other groups. As expected, the prevalence of ICH and cSS in much higher in the CAA group. The controls performed better on MoCA, memory, executive function, and processing speed compared to the other groups (all post hoc $p < 0.001$ except for controls versus MCI on processing speed where $p = 0.006$). The CAA participants performed better than AD on MoCA ($p = 0.004$), memory ($p = 0.01$), and processing speed ($p = 0.01$); however, there was no difference in executive function between these two groups. The MCI group did not differ significantly from CAA on any of the cognitive measures; however, the performance was better for MCI compared to AD on all cognitive parameters ($p < 0.001$ for MoCA, memory, and processing speed; $p = 0.007$ for executive function).

One CAA participant had hemorrhages affecting both sides of the brain and another had extremely large ventricles coupled with extensive atrophy. FreeSurfer volumetric estimation was not possible in these two cases. Participant data for smoking history (N = 2, both AD), hypertension, hypercholesterolemia, diabetes (N = 2, 1 AD, 1 MCI), memory z-score (N = 2, 1 CAA, 1 AD), executive function z-score (N = 3, 1 CAA, 2 AD) and processing speed z-score (N = 3, 2 AD, 1 MCI) were incomplete. Reasons for missing data were: participants did not complete questionnaires (N = 1), did not complete clinical visits due to COVID-19 restrictions (N = 2), withdrew from study (N = 2), or could not complete cognitive testing (N = 2).

Table 1
Summary of group characteristics.

	Controls	CAA	AD	MCI	*p*-value
N	68	32	21	26	–
Age range (years)	53–87	60–89	59–80	60–89	–
Age (years)	68.5 ± 7.2	74.6 ± 7.6	68.8 ± 6.1	72.3 ± 7.8	0.001
Education (years)	16.3 ± 3.4	13.7 ± 3.2	15.8 ± 3.2	14.8 ± 4.3	0.004
Female	44 (64.7%)	12 (37.5%)	8 (38.1%)	8 (30.8%)	0.005
Hypertension	17 (25%)	21 (65.6%)	6 (28.6%)	6 (23.1%)	< 0.001
Hypercholesterolemia	21 (30.9%)	14 (43.8%)	6 (28.6%)	11 (42.3%)	0.5
Diabetes	4 (5.9%)	3 (9.4%)	1 (4.8%)	3 (11.5%)	0.7
Current smokers	1 (1.5%)	2 (6.3%)	0 (0.0%)	1 (3.8%)	0.6
Past smokers	15 (22.1%)	17 (53.1%)	6 (28.6%)	11 (42.3%)	0.2
ICH	0 (0.0%)	4 (12.5%)	0 (0.0%)	0 (0.0%)	0.007
CMB	6 (8.8%)	30 (93.7%)	1 (4.8%)	7 (26.9%)	< 0.001
cSS	0 (0.0%)	20 (62.5%)	1 (4.8%)	0 (0.0%)	< 0.001
Focal cSS	0 (0.0%)	10 (31.3%)	1 (4.8%)	0 (0.0%)	< 0.001
Disseminated cSS	0 (0.0%)	10 (31.3%)	0 (0.0%)	0 (0.0%)	< 0.001
MoCA	26.9 ± 1.9	21.0 ± 5.4	17.5 ± 3.7	22.9 ± 3.0	< 0.001
Memory z-score	0.47 ± 1.01	−1.55 ± 1.11	−2.45 ± 0.66	−1.11 ± 1.07	< 0.001
Executive function z-score	0.48 ± 0.86	−1.26 ± 1.03	−1.76 ± 1.11	−0.75 ± 1.15	< 0.001
Processing speed z-score	0.79 ± 0.79	−0.61 ± 1.06	−1.49 ± 1.11	−0.01 ± 1.02	< 0.001

N (%) for categorical variables; mean ± SD for continuous, normally distributed variables; p-value for Chi-square and ANOVA group comparisons. The information for the rows 'Current smokers' and below are for the 47 FAVR controls and not the additional controls from the normative aging study. Abbreviations: ICH = intracerebral hemorrhage, CMB = cerebral microbleeds, cSS = cortical superficial siderosis, MoCA = Montreal Cognitive Assessment.

3.2. Subcortical brain Region, ventricle and WMH volume

FreeSurfer estimates of hippocampus, thalamus, lateral ventricle, and semi-automated estimates of WMH volumes normalized to ICV are presented in Table 2. Compared to controls, AD and MCI had smaller hippocampal (AD: −15.2%, MCI: −11.8%) and thalamic (AD: −8.7%, MCI: −8.7%) volumes. Hippocampal volumes in CAA were higher compared to AD ($p = 0.04$) and did not differ significantly from controls ($p = 0.1$) or MCI ($p = 0.3$). Lateral ventricular volumes were higher across all clinical groups (CAA: +43.9%, AD: +57.5%, MCI: +50.6%) compared to controls. WMH volumes were higher in CAA compared to all other groups ($p < 0.001$ compared to controls and MCI, $p = 0.001$ compared to AD).

3.3. Qualitative assessment of fiber tracts

Tractography of the fornix for a representative sample from each group is shown in Fig. 1. For the majority of the participants, a full 'W-shaped as viewed from above' fornix was tracked; however, 'disconnections' at the crus for streamlines from the body were observed in some cases indicating pathological change (neurodegenerative or aging), as a result of FA dropping below the tracking threshold of 0.15. Incidence of streamline disconnection was highest in participants within

Table 2
Estimated adjusted means (mean ± SD) for volumetric measures of bilateral hippocampus, thalamus, and lateral ventricles, and WMH, for control and clinical groups reported as a percentage of ICV. For the clinical groups, differences in group means, compared to controls, are reported as percentages with standard deviations. Bolded p-values indicate significant differences after FDR correction for multiple comparisons (p-corrected ≤ 0.028).

Volumes (% of ICV)	Controls	CAA	AD	MCI	*p*-value
Hippocampus	0.54 ± 0.05	0.51 ± 0.07	0.46 ± 0.08	0.48 ± 0.07	**0.004**
Δ vs Controls	–	−6.1 ± 2.7%	−15.2 ± 3.5%	−11.8 ± 2.9%	
p vs Controls	–	0.1	< 0.001	< 0.001	
Thalamus	0.92 ± 0.09	0.88 ± 0.07	0.84 ± 0.11	0.84 ± 0.08	**0.01**
Δ vs Controls	–	−4.9 ± 1.9%	−8.7 ± 2.9%	−8.7 ± 2.0%	
p vs Controls	–	0.1	0.002	0.001	
Lateral Ventricles	1.91 ± 1.00	2.75 ± 0.99	3.01 ± 1.24	2.88 ± 1.32	**0.007**
Δ vs Controls	–	43.9 ± 11.3%	57.5 ± 15.5%	50.6 ± 15.0%	
p vs Controls	–	0.004	0.001	0.001	
WMH	0.40 ± 0.40	1.91 ± 1.68	0.76 ± 0.98	0.67 ± 0.85	**0.002**
Δ vs Controls	–	374.2 ± 77.6%	89.3 ± 55.2%	67.3 ± 44.1%	
p vs Controls	–	< 0.001	0.7	0.9	
WMH – log transform	−0.66 ± 0.57	0.14 ± 0.36	−0.41 ± 0.53	−0.53 ± 0.62	**0.001**
Δ vs Controls	–	120.8 ± 15.9%	38.9 ± 21.5%	20.7 ± 22.2%	
p vs Controls	–	< 0.001	0.3	0.9	

Column of p-values corresponds to the ANOVA and rows of p-values correspond to output from post hoc comparisons (comparisons to controls only shown).

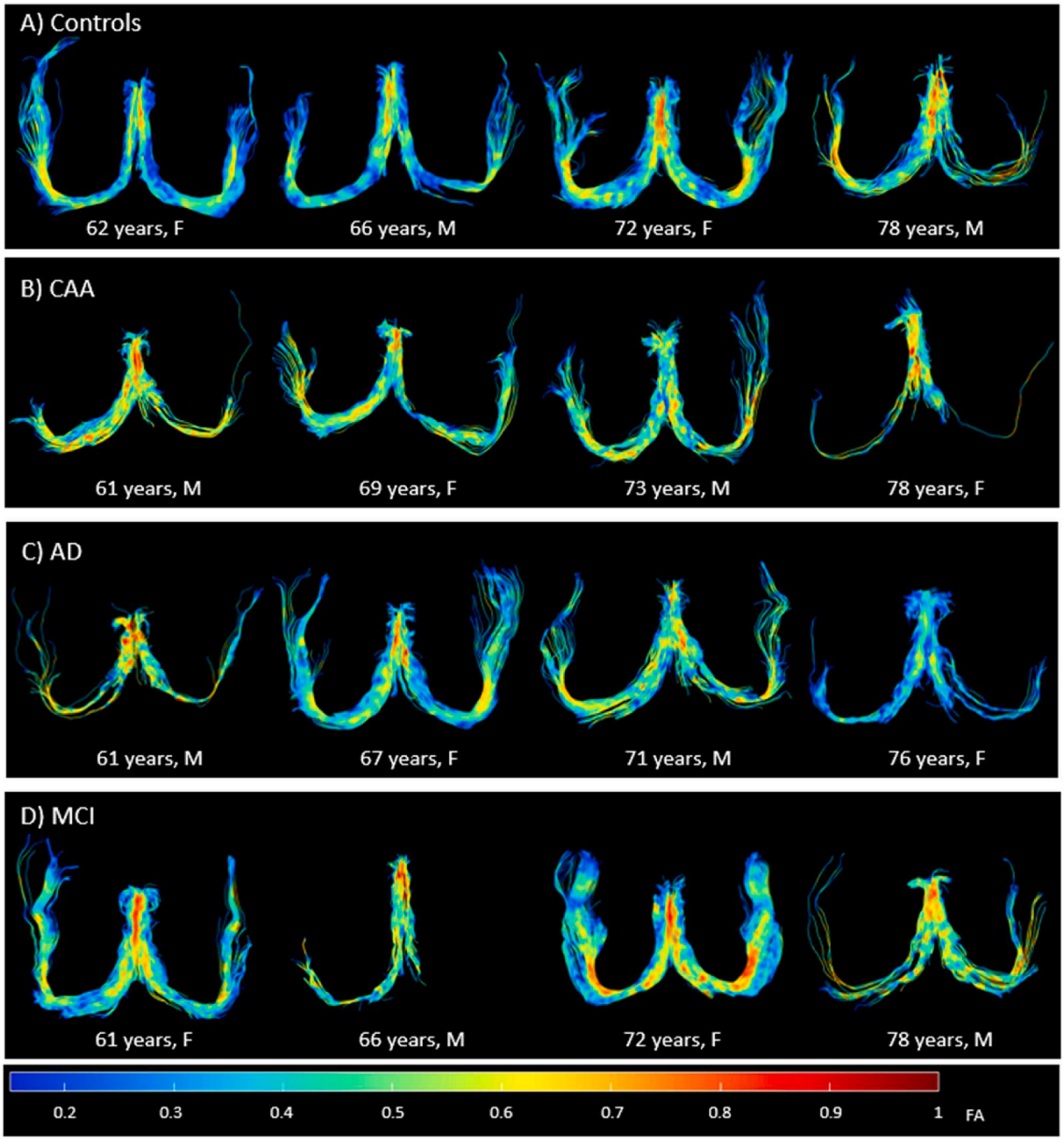

Fig. 1. Tractography of the fornix for 16 subjects (age, sex) out of the entire study cohort (n = 147) showing (A) controls, (B) CAA, (C) AD, and (D) MCI participants ordered by age and color coded by FA.

the 80–89 year age group (13 out of 19, with 1 left, 5 right, 7 bilateral), followed by substantially fewer disconnections in younger age brackets: 70–79 years (18 out of 63, with 2 left, 8 right, 8 bilateral); 60–69 years (8 out of 61 with 2 left, 5 right, 1 bilateral); and no disconnections in the 50–59 age group. Within the clinical groups, CAA had the highest number of bilateral disconnections (13 out of 32 with 1 left, 4 right, 8 bilateral), MCI had the highest incidence of disconnections (12 out of 26, 3 left, 5 right, 4 bilateral) in the crus, and AD with the least (6 out of 21, 4 right, 2 bilateral). However, as expected, controls consistently yielded fuller fornices overall with fewer disconnections (7 out of 68, 1 left, 5 right, 1 bilateral), mainly in older participants. Quantitative diffusion measures were obtained from all the residual tracts.

3.4. Fornix volume and diffusion metrics

Age-, sex-, and site-adjusted estimates of mean tract volume, MD, AXD, RD, and FA are reported in Table 3 and Fig. 2. Fornix volumes were lower for the clinical groups (CAA: −25%, AD: −30%, MCI: −26%) compared to controls, and did not differ between CAA, AD, and MCI. All measures of diffusivity were higher in AD compared to controls, with increases of 8.7% for MD, 6.4% for AXD, and 11.0% for RD ($p < 0.001$ for all comparisons). Diffusivity in CAA was also significantly higher compared to controls but to a lesser extent than for AD, with increases of 4.7% ($p = 0.04$) for MD and 4.1% ($p = 0.04$) for AXD in the CAA group. With respect to comparisons between the clinical groups, MD and RD were significantly greater in the AD participants compared to the MCI group ($p = 0.03$ for MD and $p = 0.01$ for RD). Fractional anisotropy did not differ between group overall ($p = 0.08$).

Table 3
Estimated adjusted means (mean ± standard deviation) of fornix volume and diffusion measures for control and clinical groups. For the clinical groups, differences in group means, compared to controls, are also reported as percentages with their standard deviations. Bolded p-values indicate significant differences after FDR correction for multiple comparisons (p-corrected ≤ 0.028).

Diffusion measures	Controls	CAA	AD	MCI	p-value
Tract Volume (cm^3)	4.92 ± 1.79	3.68 ± 1.89	3.44 ± 1.75	3.62 ± 1.78	**0.02**
Δ vs Controls	–	−25% ± 8%	−30% ± 9%	−26% ± 8%	
p vs Controls	–	0.02	0.006	0.02	
MD ($\times 10^{-3}$ mm^2/s)	1.10 ± 0.08	1.15 ± 0.08	1.19 ± 0.08	1.12 ± 0.08	**0.008**
Δ vs Controls	–	4.7% ± 1.6%	8.7% ± 1.8%	2.6% ± 1.8%	
p vs Controls	–	0.04	< 0.001	0.6	
AXD ($\times 10^{-3}$ mm^2/s)	1.71 ± 0.11	1.78 ± 0.12	1.82 ± 0.12	1.76 ± 0.11	**0.01**
Δ vs Controls	–	4.1% ± 1.4%	6.4% ± 1.6%	2.8% ± 1.5%	
p vs Controls	–	0.04	< 0.001	0.4	
RD (x10^{-3} mm^2/s)	0.79 ± 0.08	0.83 ± 0.08	0.88 ± 0.07	0.81 ± 0.07	**0.01**
Δ vs Controls	–	5.3% ± 2.3%	11.0% ± 2.3%	2.5% ± 2.2%	
p vs Controls	–	0.09	< 0.001	0.8	
FA	0.47 ± 0.03	0.46 ± 0.03	0.45 ± 0.03	0.47 ± 0.03	0.08
Δ vs Controls	–	−0.6% ± 1.4%	−3.6% ± 1.6%	+1% ± 1.5%	
p vs Controls	–	1	0.1	1	

The column of p-values corresponds to the ANCOVA, co-varied for age and controlled for site and sex, and rows of p-values correspond to output from post hoc pairwise comparisons.

3.5. *Volumetric and cognitive correlates of the fornix*

Pearson's partial correlation coefficients between DTI measures of the fornix and volumetric measures as well as cognitive measures across the combined patient group (CAA, AD, and MCI) are reported in Table 4. Fornix tract volume correlated positively with hippocampal ($p = 0.003$) and thalamic ($p = 0.02$) volumes and negatively with lateral ventricle volumes ($p = 0.01$). Higher diffusivity in the fornix was associated with a smaller hippocampus ($p = 0.006$ for MD, $p = 0.005$ for AXD, $p = 0.009$ for RD) and larger lateral ventricles ($p = 0.02$ for MD, $p = 0.02$ for AXD, $p = 0.02$ for RD). Thalamic volume was negatively correlated with AXD ($p = 0.03$). With respect to cognitive measures, MoCA was negatively correlated with diffusivity, with lower MoCA scores associated with greater diffusivity in the fornix ($p = 0.01$ for MD, $p = 0.02$ for AXD, $p = 0.02$ for RD). Memory z-scores positively correlated with fornix tract volume ($p = 0.02$) and negatively with diffusivity ($p = 0.02$ for MD and AXD, not significant for RD) while executive function was negatively correlated with diffusivity only ($p = 0.026$ for MD, $p = 0.027$ for AXD, not significant for RD). Fornix FA did not correlate with volumetric or cognitive measures. White matter hyperintensity volumes and processing speed were not associated with any fornix diffusion measures or tract volume. Within individual groups, diffusion measures and fornix volume did not correlate with cognitive measures. Given the small groups, this is likely a sample size issue.

4. Discussion

Differences in diffusion tensor tractography measures of the fornix were examined in patients with CAA, MCI, and AD compared to healthy controls. Using an optimized diffusion tensor tractography protocol, the main findings of this study were: 1) mean, axial and radial diffusivity of the fornix were increased in CAA and AD but not MCI compared to healthy controls while fornix tract volume was decreased in all patient groups; 2) hippocampal and thalamic volumes were comparable between CAA and controls; in contrast to MCI and AD participants where atrophy of these subcortical structures was noted; 3) ventricular dilatation was similar for all the patient groups compared to controls, suggesting global but not selective atrophy in CAA; and 4) fornix diffusion changes were associated with global cognitive impairment as well as memory and executive dysfunction, but not processing speed across these patient groups.

Previous studies have found global diffusivity changes in CAA, which were associated with white matter hyperintensities and slower processing speed (McCreary et al., 2020; Raposo et al, 2021). Global diffusivity has also been shown to be associated with pre-hemorrhage cognitive impairment (retrospectively) independent of other MR markers of CAA such as the number of microbleeds and white matter hyperintensities (Viswanathan et al., 2008). Focal changes in FA, but not diffusivity, have been reported in the splenium of the corpus callosum and temporal white matter of CAA patients (Salat et al., 2006). Cortical thinning of the occipital cortex in CAA has been shown in relation to posterior white matter connectivity using DTI tractography (Reijmer et al, 2017) while global cortical thinning is greater in CAA and is associated with memory impairment (Subotic et al., 2021). Our findings for the fornix are consistent with these previous reports of diffusivity changes in CAA as well as provide indirect evidence of global atrophy via lateral ventricle dilatation.

Studies of the fornix in aging, AD, and MCI suggest that diffusion changes in the fornix may be a sensitive early correlate of cognitive change including memory loss and executive dysfunction (Nowrangi & Rosenberg, 2015). Methodological factors may influence measurement, but changes in fornix diffusion have been found in AD compared to healthy controls (Perea et al., 2018). Diffusion changes in the fornix may act independently and synergistically with amyloid deposition to affect memory change in aging (Rabin et al., 2019). A recent study of non-amnestic memory impairment suggests fornix diffusion parameters may be correlated with executive function (Srisaikaew et al., 2020). The presence of amyloid and other markers of neurodegeneration are associated with tract specific degeneration, including in the fornix in MCI (Jacquemont et al., 2017).

The fornix is a major axonal pathway to and from the hippocampus that has been considered a target for neuro-stimulation to enhance cognitive function (Senova et al., 2020). Similar changes in diffusivity of the fornix across clinical cohorts might reflect different mechanisms. In the AD and MCI cohorts, fornix diffusivity might reflect degeneration, consistent with the greater degree of hippocampal and thalamic atrophy in these groups. In the CAA group, fornix diffusivity change may reflect axonal and myelin loss along the tracts (van Veluw et al., 2019), consistent with the observed global diffusion changes and ventricular dilatation. Our data align with the notion that relative hippocampal sparing in dementia subtypes, including AD and CAA, may reflect distinct pathologies (Ferreira et al., 2018). Our finding that both axial and radial diffusivity of the fornix correlates with hippocampus volume suggests a mechanism involving axonal and myelin degeneration of the fornix. If change to axial diffusivity is considered to be a marker for axonal injury (Song et al, 2002; Concha et al., 2006; Acosta-Cabronero and Nestor, 2014), correlates to thalamus volume could suggest specific tract loss of projections to the thalamus Longitudinal multi-modal imaging studies that include a spectrum of age-related pathologies may allow distinction of these mechanisms. Given previous findings of fornix changes in epilepsy (Campos et al., 2015), multiple sclerosis (Valdés Cabrera et al., 2020) and non-hemorrhage cerebrovascular disease (Tariq et al., 2020), multiple mechanisms may converge, affecting the fornix.

Strengths of our study included the use of CSF suppression for acquisition of diffusion images to better identify the fornix with tractography and minimize partial volume effects (Concha et al., 2005a). Prior application of FLAIR-DTI in epilepsy has shown that after eliminating CSF at acquisition, deterministic tractography identifies fornix

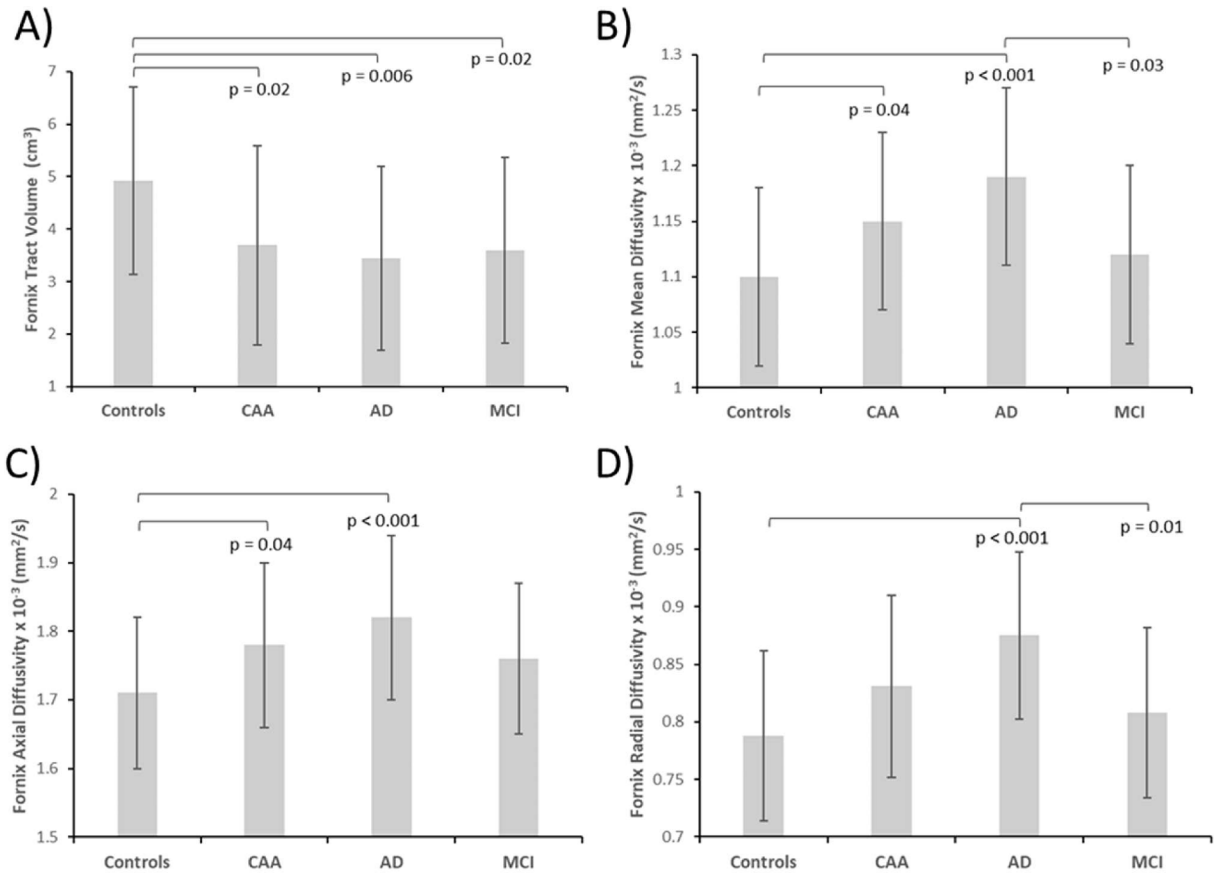

Fig. 2. Fornix diffusion measures (mean ±SD) for Controls compared to CAA, AD and MCI, showing (A) tract volume, (B) mean diffusivity, (C) axial diffusivity, and (D) radial diffusivity. Fractional diffusivity is not significantly different between all the groups and is not shown below. The p-values for between group differences for each measure are corrected post-hoc (Sidak correction).

abnormalities indicative of alterations in the axonal microstructure (Concha et al, 2005b). Moreover, the changes noted were consistent within cohorts at each of the two sites and our global analyses included site as a covariate. We used standardized clinical criteria with patients meeting criteria for probable CAA, AD and MCI. Furthermore, controls were screened for the presence of cognitive impairment using standardized testing.

Some limitations of our study include the relatively small sample size that might have reduced our ability to identify distinct neuropsychological correlates of fornix atrophy within the groups. Moreover, the small sample size limited our ability to examine specific patterns of CAA change, such as the presence of cortical superficial siderosis or tau pathology which might affect atrophy (Kim et al., 2018; Schoemaker et al., 2021). Ideally, we would have had identical scan acquisition protocols in a multi-site study; however, this is impractical given different scanners were used at the different centres. Combining data from two sites strengthened our group analysis due to greater total and subgroup sample sizes. The major difference between FLAIR-DTI protocols across sites was the in-plane voxel resolution and differences in MRI scanner hardware differences across sites (vendor, coils). Nevertheless, the fornix volume and diffusion parameters of travelling heads, and the overall data trends for all the participants between sites were similar. We also focussed on a single tract with importance in cognition. Individual fiber tracking is labour intensive but affords best tract identification for each participant. We focussed on cognitive correlates and did not examine neuropsychiatric correlates of fornix changes, which may be clinically important. We also averaged DTI measures across the entire fornix rather than separating the right and left which might affect clinical correlations. While we restricted our study to patients with probable CAA based on the Boston Criteria (Charidimou et al., 2017) and AD and MCI based on established criteria (Chertkow et al., 2019), there remains a possibility of misdiagnosis, given the lack of autopsy confirmation.

Combining the participants from all four groups, there was a lack of a fully tracked fornix in 39 individuals which was mainly evident in older individuals including 13% of the 60–69 year old group, 28% of the 70–79 year old group, and 68% of the 80–89 year old group. The deterministic tractography methodology utilized to track the fornix stops tracking when a voxel falls below an FA threshold. Fewer or truncated streamlines resulting from poor tractography indicates tract degradation which worsen with aging and pathology. We recognize that this is an underestimate of the true fornix volume, but when it happens it does highlight that volume and/or microstructure is abnormal. Nevertheless, a partially reconstructed tract does not mean that there is no biological pathway in that area nor that the physical fornix bundle is in fact transected. Tractography stops in those areas because the FA threshold (or angle of eigenvectors between adjacent voxels threshold) was not reached, despite the suppression of isotropic CSF and increased voxel resolution when compared to previous FLAIR-DTI acquisitions for the fornix (Concha et al., 2005a,b).

The fornix has major connections to the hippocampus relevant to cognition in aging and neurodegenerative disorders. Our current study indicates that it is additionally affected in CAA. Given highly reliable methods that can be applied across centers, our methods offer the potential to examine diffusion parameters in the fornix as an outcome measure. Potential differences in pathophysiology (degeneration versus vascular changes) suggest that different approaches to preventing neurodegeneration of the fornix, or combined approaches, might be needed in the context of parenchymal (AD) versus vascular (CAA) amyloid pathology. The fornix has also been examined as a target for

Table 4
Correlates of fornix tract volume/diffusion measures with other subcortical volumes (normalized to ICV) and cognitive measures over the combined patient group (CAA, AD and MCI). Partial correlation coefficients, R, reported followed by *p*-values reported in brackets. Bolded p-values indicate significant correlations after FDR correction (p-corrected $\leq$ 0.028) for multiple comparisons. Correlations controlled for age, sex, and site for volumetric and cognitive measures, and additionally controlled for years of education for cognitive measures.

	R(p) – Tract Volume	R(p) – MD	R(p) – AXD	R(p) – RD	R(p) – FA
Hippocampal volume (% ICV)	0.558 (**0.003**)	−0.507 (**0.006**)	−0.513 (**0.005**)	−0.451 (**0.009**)	0.098 (0.4)
Thalamus volume (% ICV)	0.362 (**0.02**)	−0.229 (0.05)	−0.277 (**0.03**)	0.170 (0.1)	−0.084 (0.5)
Lateral ventricles volume (% ICV)	−0.406 (**0.01**)	0.380 (**0.02**)	0.376 (**0.02**)	0.344 (**0.02**)	−0.032 (0.8)
WMH (% ICV)	−0.061 (0.6)	−0.048 (0.7)	0.007 (1)	−0.084 (0.5)	0.152 (0.2)
WMH (%ICV) – log transformed	−0.087 (0.5)	−0.008 (0.9)	0.081 (0.5)	−0.074 (0.5)	0.200 (0.09)
MoCA	0.190 (0.1)	−0.336 (**0.01**)	−0.306 (**0.02**)	−0.319 (**0.02**)	0.103 (0.4)
Memory z-score	0.293 (**0.02**)	−0.298 (**0.02**)	−0.306 (**0.02**)	−0.26 (0.031)	0.046 (0.7)
Executive z-score	0.226 (0.06)	−0.286 (**0.026**)	−0.278 (**0.027**)	−0.26 (0.031)	0.056 (0.6)
Processing speed z-score	0.126 (0.3)	−0.203 (0.09)	−0.209 (0.08)	−0.176 (0.1)	−0.009 (0.9)

neuromodulation making methods for its accurate measurement relevant.

In conclusion, microstructural changes in the fornix occur in probable CAA, without corresponding hippocampal or thalamic atrophy, likely reflecting axonal damage and demyelination. Moreover, we confirm that diffusion changes in the fornix are evident in AD and to a lesser extent in MCI, where we observed hippocampal and thalamic atrophy. Given the importance of the fornix as a major white matter pathway to and from the hippocampus and demonstration in the literature that it is impacted in a number of neurological diseases, its prognostic and clinical correlates require further exploration in CAA. Our acquisition can be applied across sites and tractography based on this method should be explored in additional tracts adjacent to CSF, such as the uncinate fasciculus among others (Salminen et al., 2016). Additional studies examining the specificity of the fornix changes are necessary.

Funding

This work was supported by the Canadian Consortium on Neurodegeneration of Aging (CIHR and partners: CCNA 137794, https://www.ccna-ccnv.ca) and the Canadian Institutes of Health Research (Grant # MOP-142175 and FDN-154317), Brain Canada, Canadian Stroke Network (Grant #MIRI2015-3994), Heart and Stroke Foundation of Alberta and the Alzheimer Society of Canada.

CB is supported by the Canada Research Chairs program.

Declaration of Competing Interest

The authors declare that they have no known competing financial interests or personal relationships that could have appeared to influence the work reported in this paper.

Acknowledgements

We are grateful to all the participants who volunteered for this study. We would also like to acknowledge Anna Charlton and Angela Zwiers for study coordination in Calgary, and Krista Nelles and Jacqueline Burt for study coordination in Edmonton. Assistance from Dr. Michael Martyna in the early stages of this project is much appreciated.

References

Acosta-Cabronero, J., Nestor, P.J., 2014. Diffusion tensor imaging in Alzheimer's disease: insights into the limbic-diencephalic network and methodological considerations. Front. Aging Neurosci. 2 (6), 266. https://doi.org/10.3389/fnagi.2014.00266. PMID: 25324775; PMCID: PMC4183111.

Albert, M.S., DeKosky, S.T., Dickson, D., Dubois, B., Feldman, H.H., Fox, N.C., Gamst, A., Holtzman, D.M., Jagust, W.J., Petersen, R.C., Snyder, P.J., Carrillo, M.C., Thies, B., Phelps, C.H., 2011. The diagnosis of mild cognitive impairment due to Alzheimer's disease: recommendations from the National Institute on Aging-Alzheimer's Association workgroups on diagnostic guidelines for Alzheimer's disease. Alzheimers Dement. 7 (3), 270–279. https://doi.org/10.1016/j.jalz.2011.03.008. Epub 2011 Apr 21. PMID: 21514249; PMCID: PMC3312027.

Benedictus, M.R., Goos, J.D., Binnewijzend, M.A., Muller, M., Barkhof, F., Scheltens, P., Prins, N.D., van der Flier, W.M., 2013. Specific risk factors for microbleeds and white matter hyperintensities in Alzheimer's disease. Neurobiol. Aging 34 (11), 2488–2494. https://doi.org/10.1016/j.neurobiolaging.2013.04.023. Epub 2013 May 31 PMID: 23731952.

Campos, B.M., Coan, A.C., Beltramini, G.C., Liu, M., Yassuda, C.L., Ghizoni, E., Beaulieu, C., Gross, D.W., Cendes, F., 2015. White matter abnormalities associate with type and localization of focal epileptogenic lesions. Epilepsia. 56 (1), 125–132. https://doi.org/10.1111/epi.12871. Epub 2014 Dec 26 PMID: 25545559.

Case, N.F., Charlton, A., Zwiers, A., Batool, S., McCreary, C.R., Hogan, D.B., Ismail, Z., Zerna, C., Coutts, S.B., Frayne, R., Goodyear, B., Haffenden, A., Smith, E.E., 2016. Cerebral amyloid angiopathy is associated with executive dysfunction and mild cognitive impairment. Stroke 47 (8), 2010–2016. https://doi.org/10.1161/STROKEAHA.116.012999. Epub 2016 Jun 23 PMID: 27338926.

Charidimou, A., Boulouis, G., Gurol, M.E., Ayata, C., Bacskai, B.J., Frosch, M.P., Viswanathan, A., Greenberg, S.M., 2017. Emerging concepts in sporadic cerebral amyloid angiopathy. Brain 140 (7), 1829–1850. https://doi.org/10.1093/brain/awx047. PMID: 28334869; PMCID: PMC6059159.

Chertkow, H., Borrie, M., Whitehead, V., Black, S.E., Feldman, H.H., Gauthier, S., Hogan, D.B., Masellis, M., McGilton, K., Rockwood, K., Tierney, M.C., Andrew, M., Hsiung, G.R., Camicioli, R., Smith, E.E., Fogarty, J., Lindsay, J., Best, S., Evans, A., Das, S., Mohaddes, Z., Pilon, R., Poirier, J., Phillips, N.A., MacNamara, E., Dixon, R. A., Duchesne, S., MacKenzie, I., Rylett, R.J., 2019. The comprehensive assessment of neurodegeneration and dementia: canadian cohort study. Can. J. Neurol. Sci. 46 (5), 499–511. https://doi.org/10.1017/cjn.2019.27. Epub 2019 Jul 16 PMID: 31309917.

Concha, L., Gross, D.W., Beaulieu, C., 2005a. Diffusion tensor tractography of the limbic system. AJNR Am J Neuroradiol. 26 (9), 2267–2274. PMID: 16219832; PMCID: PMC7976161.

Concha, L., Beaulieu, C., Gross, D.W., 2005b. Bilateral limbic diffusion abnormalities in unilateral temporal lobe epilepsy. Ann Neurol. 57 (2), 188–196. https://doi.org/10.1002/ana.20334. PMID: 15562425.

Concha, L., Gross, D.W., Wheatley, B.M., Beaulieu, C., 2006. Diffusion tensor imaging of time-dependent axonal and myelin degradation after corpus callosotomy in epilepsy patients. Neuroimage. 32 (3), 1090–1099. https://doi.org/10.1016/j.neuroimage.2006.04.187. Epub 2006 Jun 9. PMID: 16765064.

Duchesne, S., Chouinard, I., Potvin, O., Fonov, V.S., Khademi, A., Bartha, R., Bellec, P., Collins, D.L., Descoteaux, M., Hoge, R., McCreary, C.R., Ramirez, J., Scott, C.J.M., Smith, E.E., Strother, S.C., Black, S.E., 2019. CIMA-Q group and the CCNA group. The Canadian Dementia Imaging Protocol: Harmonizing National Cohorts. J. Magn. Reson Imaging 49 (2), 456–465. https://doi.org/10.1002/jmri.26197. PMID: 30635988.

Ferreira, D., Shams, S., Cavallin, L., Viitanen, M., Martola, J., Granberg, T., Shams, M., Aspelin, P., Kristoffersen-Wiberg, M., Nordberg, A., Wahlund, L.O., Westman, E., 2018 Oct. The contribution of small vessel disease to subtypes of Alzheimer's disease: a study on cerebrospinal fluid and imaging biomarkers. Neurobiol Aging. 70, 18–29. https://doi.org/10.1016/j.neurobiolaging.2018.05.028. Epub 2018 May 30. PMID: 29935417.

Fischl B. FreeSurfer. Neuroimage. 2012 Aug 15;62(2):774-81. doi: 10.1016/j.neuroimage.2012.01.021. Epub 2012 Jan 10. PMID: 22248573; PMCID: PMC3685476.

Fletcher, E., Raman, M., Huebner, P., Liu, A., Mungas, D., Carmichael, O., DeCarli, C., 2013. Loss of fornix white matter volume as a predictor of cognitive impairment in cognitively normal elderly individuals. JAMA Neurol. 70 (11), 1389–1395. https://doi.org/10.1001/jamaneurol.2013.3263. PMID: 24018960; PMCID: PMC4059679.

Fotiadis P, van Rooden S, van der Grond J, Schultz A, Martinez-Ramirez S, Auriel E, Reijmer Y, van Opstal AM, Ayres A, Schwab KM; Alzheimer's Disease Neuroimaging Initiative, Hedden T, Rosand J, Viswanathan A, Wermer M, Terwindt G, Sperling RA, Polimeni JR, Johnson KA, van Buchem MA, Greenberg SM, Gurol ME. Cortical atrophy in patients with cerebral amyloid angiopathy: a case-control study. Lancet Neurol. 2016 Jul;15(8):811-819. doi: 10.1016/S1474-4422(16)30030-8. Epub 2016 May 11. PMID: 27180034; PMCID: PMC5248657.

Fotiadis P, Reijmer YD, Van Veluw SJ, Martinez-Ramirez S, Karahanoglu FI, Gokcal E, Schwab KM; Alzheimer's Disease Neuroimaging Initiative study group, Goldstein JN, Rosand J, Viswanathan A, Greenberg SM, Gurol ME. White matter atrophy in cerebral amyloid angiopathy. Neurology. 2020 Aug 4;95(5):e554-e562. doi: 10.1212/WNL.0000000000010017. Epub 2020 Jul 1. PMID: 32611644; PMCID: PMC7455340.

Greenberg SM, Charidimou A. Diagnosis of Cerebral Amyloid Angiopathy: Evolution of the Boston Criteria. Stroke. 2018 Feb;49(2):491-497. doi: 10.1161/STROKEAHA.117.016990. Epub 2018 Jan 15. PMID: 29335334; PMCID: PMC5892842.

Greenberg, S.M., Rebeck, G.W., Vonsattel, J.P., Gomez-Isla, T., Hyman, B.T., 1995. Apolipoprotein E epsilon 4 and cerebral hemorrhage associated with amyloid angiopathy. Ann. Neurol. 38 (2), 254–259. https://doi.org/10.1002/ana.410380219. PMID: 7654074.

Jacquemont T, De Vico Fallani F, Bertrand A, Epelbaum S, Routier A, Dubois B, Hampel H, Durrleman S, Colliot O; Alzheimer's Disease Neuroimaging Initiative. Amyloidosis and neurodegeneration result in distinct structural connectivity patterns in mild cognitive impairment. Neurobiol Aging. 2017 Jul;55:177-189. doi: 10.1016/j.neurobiolaging.2017.03.023. Epub 2017 Apr 5. PMID: 28457579.

Kim, J., Na, H.K., Shin, J.H., Kim, H.J., Seo, S.W., Seong, J.K., Na, D.L., 2018. Atrophy patterns in cerebral amyloid angiopathy with and without cortical superficial siderosis. Neurology. 90 (20), e1751–e1758. https://doi.org/10.1212/WNL.0000000000005524. Epub 2018 Apr 20 PMID: 29678935.

Knopman DS, Jack CR Jr, Lundt ES, Weigand SD, Vemuri P, Lowe VJ, Kantarci K, Gunter JL, Senjem ML, Mielke MM, Machulda MM, Roberts RO, Boeve BF, Jones DT, Petersen RC. Evolution of neurodegeneration-imaging biomarkers from clinically normal to dementia in the Alzheimer disease spectrum. Neurobiol Aging. 2016 Oct;46:32-42. doi: 10.1016/j.neurobiolaging.2016.06.003. Epub 2016 Jun 16. PMID: 27460147; PMCID: PMC5018437.

Kwong KK, McKinstry RC, Chien D, Crawley AP, Pearlman JD, Rosen BR. CSF-suppressed quantitative single-shot diffusion imaging. Magn Reson Med. 1991 Sep;21(1):157-63. doi: 10.1002/mrm.1910210120. PMID: 1943674.

Leemans, A.J., Jeurissen, B., Sijbers, J., Jones, D.K., 2009. ExploreDTI: a graphical toolbox for Processing, analyzing, and visualizing diffusion MR data. Proc. Int. Soc. Magn. Reson. Med. 17, 3537.

Linn, J., Halpin, A., Demaerel, P., Ruhland, J., Giese, A.D., Dichgans, M., van Buchem, M. A., Bruckmann, H., Greenberg, S.M., 2010. Prevalence of superficial siderosis in patients with cerebral amyloid angiopathy. Neurology 74 (17), 1346–1350. https://doi.org/10.1212/WNL.0b013e3181dad605. PMID: 20421578; PMCID: PMC2875936.

McCreary CR, Beaudin AE, Subotic A, Zwiers AM, Alvarez A, Charlton A, Goodyear BG, Frayne R, Smith EE. Cross-sectional and longitudinal differences in peak skeletonized white matter mean diffusivity in cerebral amyloid angiopathy. Neuroimage Clin. 2020;27:102280. doi: 10.1016/j.nicl.2020.102280. Epub 2020 May 26. PMID: 32521475; PMCID: PMC7284130.

McKhann, G.M., 2011. Changing concepts of Alzheimer disease. JAMA 305 (23), 2458–2459. https://doi.org/10.1001/jama.2011.810. PMID: 21673298.

McKhann GM, Knopman DS, Chertkow H, Hyman BT, Jack CR Jr, Kawas CH, Klunk WE, Koroshetz WJ, Manly JJ, Mayeux R, Mohs RC, Morris JC, Rossor MN, Scheltens P, Carrillo MC, Thies B, Weintraub S, Phelps CH. The diagnosis of dementia due to Alzheimer's disease: recommendations from the National Institute on Aging-Alzheimer's Association workgroups on diagnostic guidelines for Alzheimer's disease. Alzheimers Dement. 2011 May;7(3):263-9. doi: 10.1016/j.jalz.2011.03.005. Epub 2011 Apr 21. PMID: 21514250; PMCID: PMC3312024.

Nowrangi, M.A., Rosenberg, P.B., 2015. The fornix in mild cognitive impairment and Alzheimer's disease. Front. Aging Neurosci. 21 (7), 1. https://doi.org/10.3389/fnagi.2015.00001. PMID: 25653617; PMCID: PMC4301006.

Peca S, McCreary CR, Donaldson E, Kumarpillai G, Shobha N, Sanchez K, Charlton A, Steinback CD, Beaudin AE, Flück D, Pillay N, Fick GH, Poulin MJ, Frayne R, Goodyear BG, Smith EE. Neurovascular decoupling is associated with severity of cerebral amyloid angiopathy. Neurology. 2013 Nov 5;81(19):1659-65. doi: 10.1212/01.wnl.0000435291.49598.54. Epub 2013 Oct 4. PMID: 24097810; PMCID: PMC3812103.

Perea RD, Rabin JS, Fujiyoshi MG, Neal TE, Smith EE, Van Dijk KRA, Hedden T. Connectome-derived diffusion characteristics of the fornix in Alzheimer's disease. Neuroimage Clin. 2018 Apr 27;19:331-342. doi: 10.1016/j.nicl.2018.04.029. PMID: 30013916; PMCID: PMC6044183.

Potvin O, Chouinard I, Dieumegarde L, Bartha R, Bellec P, Collins DL, Descoteaux M, Hoge R, Ramirez J, Scott CJM, Smith EE, Strother SC, Black SE, Duchesne S; CIMA-Q group; CCNA group. The Canadian Dementia Imaging Protocol: Harmonization validity for morphometry measurements. Neuroimage Clin. 2019;24:101943. doi: 10.1016/j.nicl.2019.101943. Epub 2019 Jul 18. PMID: 31351228; PMCID: PMC6661407.

Rabin JS, Perea RD, Buckley RF, Johnson KA, Sperling RA, Hedden T. Synergism between fornix microstructure and beta amyloid accelerates memory decline in clinically normal older adults. Neurobiol Aging. 2019 Sep;81:38-46. doi: 10.1016/j.neurobiolaging.2019.05.005. Epub 2019 May 16. PMID: 31207468; PMCID: PMC6732225.

Raposo N, Zanon Zotin MC, Schoemaker D, Xiong L, Fotiadis P, Charidimou A, Pasi M, Boulouis G, Schwab K, Schirmer MD, Etherton MR, Gurol ME, Greenberg SM, Duering M, Viswanathan A. Peak Width of Skeletonized Mean Diffusivity as Neuroimaging Biomarker in Cerebral Amyloid Angiopathy. AJNR Am J Neuroradiol. 2021 May;42(5):875-881. doi: 10.3174/ajnr.A7042. Epub 2021 Mar 4. PMID: 33664113; PMCID: PMC8115367.

Reijmer YD, Fotiadis P, Riley GA, Xiong L, Charidimou A, Boulouis G, Ayres AM, Schwab K, Rosand J, Gurol ME, Viswanathan A, Greenberg SM. Progression of Brain Network Alterations in Cerebral Amyloid Angiopathy. Stroke. 2016 Oct;47(10):2470-5. doi: 10.1161/STROKEAHA.116.014337. Epub 2016 Aug 30. PMID: 27576378; PMCID: PMC5039080.

Reijmer YD, Fotiadis P, Charidimou A, van Veluw SJ, Xiong L, Riley GA, Martinez-Ramirez S, Schwab K, Viswanathan A, Gurol ME, Greenberg SM. Relationship between white matter connectivity loss and cortical thinning in cerebral amyloid angiopathy. Hum Brain Mapp. 2017 Jul;38(7):3723-3731. doi: 10.1002/hbm.23629. Epub 2017 Apr 30. PMID: 28462514; PMCID: PMC5662494.

Salat, D.H., Smith, E.E., Tuch, D.S., Benner, T., Pappu, V., Schwab, K.M., Gurol, M.E., Rosas, H.D., Rosand, J., Greenberg, S.M., 2006. White matter alterations in cerebral amyloid angiopathy measured by diffusion tensor imaging. Stroke 37 (7), 1759–1764. https://doi.org/10.1161/01.STR.0000227328.86353.a7. Epub 2006 Jun 8 PMID: 16763176.

Salminen LE, Conturo TE, Bolzenius JD, Cabeen RP, Akbudak E, Paul RH. Reducing CSF Partial Volume Effects to Enhance Diffusion Tensor Imaging Metrics of Brain Microstructure. Technol Innov. 2016 Apr;18(1):5-20. doi: 10.21300/18.1.2016.5. Epub 2016 Apr 1. PMID: 27721931; PMCID: PMC5054978.

Schoemaker D, Charidimou A, Zanon Zotin MC, Raposo N, Johnson KA, Sanchez JS, Greenberg SM, Viswanathan A. Association of Memory Impairment With Concomitant Tau Pathology in Patients With Cerebral Amyloid Angiopathy. Neurology. 2021 Apr 13;96(15):e1975-e1986. doi: 10.1212/WNL.0000000000011745. Epub 2021 Feb 24. PMID: 33627498; PMCID: PMC8166424.

Senova S, Fomenko A, Gondard E, Lozano AM. Anatomy and function of the fornix in the context of its potential as a therapeutic target. J Neurol Neurosurg Psychiatry. 2020 May;91(5):547-559. doi: 10.1136/jnnp-2019-322375. Epub 2020 Mar 4. PMID: 32132227; PMCID: PMC7231447.

Smith EE, Duchesne S, Gao F, Saad F, Whitehead V, McCreary CR, Frayne R, Gauthier S, Camicioli R, Borrie M, Black SE. Vascular Contributions to Neurodegeneration: Protocol of the COMPASS-ND Study. Can J Neurol Sci. 2021 Jan 28:1-8. doi: 10.1017/cjn.2021.19. Epub ahead of print. PMID: 33504400.

Song, S.K., Sun, S.W., Ramsbottom, M.J., Chang, C., Russell, J., Cross, A.H., 2002. Dysmyelination revealed through MRI as increased radial (but unchanged axial) diffusion of water. Neuroimage. 17 (3), 1429–1436. https://doi.org/10.1006/nimg.2002.1267. PMID: 12414282.

Srisaikaew, P., Wongpakaran, N., Anderson, N.D., Chen, J.J., Kothan, S., Varnado, P., Unsrisong, K., Mahakkanukrauh, P., 2020. Fornix integrity is differently associated with cognition in healthy aging and non-amnestic mild cognitive impairment: a pilot diffusion tensor imaging study in thai older adults. Front. Aging Neurosci. 2 (12), 594002 https://doi.org/10.3389/fnagi.2020.594002. PMID: 33343334; PMCID: PMC7745667.

Subotic, A., McCreary, C.R., Saad, F., Nguyen, A., Alvarez-Veronesi, A., Zwiers, A.M., Charlton, A., Beaudin, A.E., Ismail, Z., Pike, G.B., Smith, E.E., 2021. Cortical thickness and its association with clinical cognitive and neuroimaging markers in cerebral amyloid angiopathy. J. Alzheimers Dis. 81 (4), 1663–1671. https://doi.org/10.3233/JAD-210138. PMID: 33998545.

Tang, S.X., Feng, Q.L., Wang, G.H., Duan, S., Shan, B.C., Dai, J.P., 2017. Diffusion characteristics of the fornix in patients with Alzheimer's disease. Psychiatry Res Neuroimag. 30 (265), 72–76. https://doi.org/10.1016/j.pscychresns.2016.09.012. Epub 2016 Oct 1 PMID: 28017479.

Tariq, S., Tsang, A., Wang, M., Reaume, N., Carlson, H., Sajobi, T.T., Longman, R.S., Smith, E.E., Frayne, R., d'Esterre, C.D., Coutts, S.B., Barber, P.A., 2020. White matter tract microstructure and cognitive performance after transient ischemic attack. PLoS ONE 15 (10), e0239116. https://doi.org/10.1371/journal.pone.0239116. PMID: 33095770; PMCID: PMC7584182.

Valdés Cabrera D, Stobbe R, Smyth P, Giuliani F, Emery D, Beaulieu C. Diffusion tensor imaging tractography reveals altered fornix in all diagnostic subtypes of multiple sclerosis. Brain Behav. 2020 Jan;10(1):e01514. doi: 10.1002/brb3.1514. Epub 2019 Dec 19. PMID: 31858742; PMCID: PMC6955822.

van Veluw SJ, Reijmer YD, van der Kouwe AJ, Charidimou A, Riley GA, Leemans A, Bacskai BJ, Frosch MP, Viswanathan A, Greenberg SM. Histopathology of diffusion imaging abnormalities in cerebral amyloid angiopathy. Neurology. 2019 Feb 26;92(9):e933-e943. doi: 10.1212/WNL.0000000000007005. Epub 2019 Jan 30. PMID: 30700595; PMCID: PMC6404469.

Viswanathan A, Patel P, Rahman R, Nandigam RN, Kinnecom C, Bracoud L, Rosand J, Chabriat H, Greenberg SM, Smith EE. Tissue microstructural changes are independently associated with cognitive impairment in cerebral amyloid angiopathy. Stroke. 2008 Jul;39(7):1988-92. doi: 10.1161/STROKEAHA.107.509091. Epub 2008 Apr 24. PMID: 18436874; PMCID: PMC2698787.

Wardlaw JM, Smith EE, Biessels GJ, Cordonnier C, Fazekas F, Frayne R, Lindley RI, O'Brien JT, Barkhof F, Benavente OR, Black SE, Brayne C, Breteler M, Chabriat H, Decarli C, de Leeuw FE, Doubal F, Duering M, Fox NC, Greenberg S, Hachinski V, Kilimann I, Mok V, Oostenbrugge Rv, Pantoni L, Speck O, Stephan BC, Teipel S, Viswanathan A, Werring D, Chen C, Smith C, van Buchem M, Norrving B, Gorelick PB, Dichgans M; STandards for ReportIng Vascular changes on nEuroimaging (STRIVE v1). Neuroimaging standards for research into small vessel disease and its contribution to ageing and neurodegeneration. Lancet Neurol. 2013 Aug;12(8):822-38. doi: 10.1016/S1474-4422(13)70124-8. PMID: 23867200; PMCID: PMC3714437.

Xiong, L., Davidsdottir, S., Reijmer, Y.D., Shoamanesh, A., Roongpiboonsopit, D., Thanprasertsuk, S., Martinez-Ramirez, S., Charidimou, A., Ayres, A.M., Fotiadis, P., Gurol, E., Blacker, D.L., Greenberg, S.M., Viswanathan, A., 2016. Cognitive profile and its association with neuroimaging markers of non-demented cerebral amyloid angiopathy patients in a stroke unit. J. Alzheimers Dis. 52 (1), 171–178. https://doi.org/10.3233/JAD-150890. PMID: 27060947.